INL/CON-15-37504
PREPRINT

Heat Transfer Model of a Small-Scale Waste Glass Melter with Cold Cap Layer

11th International Topical Meeting on Nuclear Thermal Hydraulics, Operation and Safety

Alexander Abboud, Donna Post Guillen, Richard Pokorny

September 2016

The INL is a
U.S. Department of Energy
National Laboratory
operated by
Battelle Energy Alliance

Heat Transfer Model of a Small-Scale Waste Glass Melter with Cold Cap Layer

Alexander Abboud, Donna Post Guillen
Idaho National Laboratory
Idaho Falls, ID 83415
Alexander.Abboud@inl.gov, Donna.Guillen@inl.gov

Richard Pokorny
University of Chemistry and Technology Prague
Czech Republic
Richard.Pokorny@vscht.com

ABSTRACT

At the Hanford site in the state of Washington, more than 56 million gallons of radioactive waste are stored in underground tanks. The cleanup plan for this waste is vitrification at the Waste Treatment Plant (WTP), currently under construction. At the WTP, the waste will be blended with glass-forming materials and heated to 1423K, then poured into stainless steel canisters to cool and solidify. A fundamental understanding of the glass batch melting process is needed to optimize the process to reduce cost and decrease the life cycle of the cleanup effort. The cold cap layer that floats on the surface of the glass melt is the primary zone for the feed-to-glass conversion. Among other physics, the conversion process includes water release, melting of salts, evolution of batch gases, dissolution of quartz and the formation of molten glass. Obtaining efficient heat transfer to this region is crucial to achieving high rates of glass conversion. Computational multiphase fluid dynamics (CMFD) modeling is being used to understand the heat transfer dynamics of the system and provide insight to optimize the process. A CMFD model was developed to simulate the DM100, a small-scale melter that has been extensively tested by the Vitreous State Laboratory (VSL). Electrodes are built into the melter to provide Joule heating to the molten glass. To promote heat transfer from the molten glass into the reactive cold cap layer, bubbling of the molten glass is used to stimulate forced convection within the melt pool. A three-phase volume of fluid approach is utilized to model the system, wherein the molten glass and cold cap regions are modeled as separate liquid phases, and the bubbling gas and plenum regions are modeled as one lumped gas phase. The modeling of the entire system with a volume of fluid approach allows for the prescription of physical properties on a per-phase basis. The molten glass phase and the gas phase physical properties are obtained from previous experimental work. Determining representative properties for the cold cap region is more difficult, as this region is not a true liquid, but rather a multilayer region consisting of a porous and a foamy layer. In this paper, the effect of bubbling on the molten glass/cold cap interface are assessed. These results will serve to inform improved models of the cold cap with the ultimate goal of increasing melt rate and throughput of the melter.

KEYWORDS

Glass Waste Melter Model, Waste Vitrification, Hanford Tank Waste

1. INTRODUCTION

At the Hanford site in the state of Washington, Joule-heated ceramic lined waste glass melters are being installed at the Hanford Waste Treatment Plant (WTP) for vitrification of legacy radioactive waste. Waste slurry consisting of radioactive waste and glass forming compounds is fed into the melter

from above and heated to produce a stable solid, glass waste form for disposal. Electrodes are immersed in the melter on opposite sides of the tank and the electrical current between the electrodes is dissipated as heat into the glass phase. This heat supplies energy for the feed-to-glass conversation reactions that occur in the cold cap, the layer of reacting feed that floats on the heated glass [1]. The region above the cold cap consists of a large plenum where reaction gases and bubbling air are vented before being funneled to the off-gas system.

The Vitreous State Laboratory (VSL) at the Catholic University of America has conducted experiments of various melter configurations and scales in order to understand the dynamics of these types of systems. These studies have ranged from variations of the waste feed simulant streams, adjusting the bubbler configurations and flow rates, and studying the effect of spinel formation as melting occurs [2-7]. Experiments have also been conducted on inert flows of viscous fluids [8], the results of which have been used for validation of an isothermal, inert bubbling CMFD model [9]. The experiments at VSL have varied in the size of the studies from small-scale batch crucible melts, to a small-scale Joule heated melter (the DM100), up to the high level waste pilot-scale melter (the DM1200) [7]. Using gas bubblers in production melter systems has been shown to significantly increase the glass production rate by improving the heat transfer from the molten glass into the cold cap region [10]. The incorporation of bubblers is common throughout the experimental tests at VSL.

The main reactions that convert the feed simulant into glass occur in the cold cap region. The cold cap is a foamy region that is mainly comprised of the tank slurry and glass formers fed from the top of the melter [11]. Understanding the physical characteristics and behavior of the cold cap is important to model heat transfer effects to this region, and subsequently the reaction rates of the feed simulant. Previous studies have used temperature data from batch melts in order to calculate the physical characteristics of the cold cap in a one-dimensional model, including bulk properties for the thermal conductivity, density and viscosity of the cold cap [12-14]. Thermogravimetric and evolved gas analysis of feed pellets has also been conducted to construct models for the evolution of gas [15,16] as well as modeling the heat capacity of the cold cap phase [17].

A computational multiphase fluid dynamics (CMFD) model of the melter is being developed to provide an understanding of the complex, interrelated processes occurring within the waste glass melters [18]. A high-fidelity representation of the cold cap coupled with the three-dimensional mass and heat flow modeled using CMFD can give an accurate assessment of the forced convection currents which occur due to the bubbling [2]. The development of a rigorous melter model will provide a basis for optimization of the heat transfer into the cold cap due to convection and conduction, thus improve the previous modeling efforts [19]. Enhanced convective transport in the glass pool increases the heat transfer to the cold cap region leading to higher glass conversion rates as evidenced by experiments [3].

To determine the most appropriate modeling framework, characteristic information about the fluid regime is required. For the melter application discussed in this study, it has been well documented in experimental studies that the injected air phase forms large bubbles in the molten glass phase [2-6,8]. These bubbles are large enough that Lagrangian approaches are not applicable, and the use of an Eulerian multiphase technique is required. These large bubbles significantly disrupt the free surface at the fluid interface, which requires a free surface wave solution for the Navier-Stokes equations. Two categories for solving this type of flow are interface tracking and interface-capturing methods. Interface-tracking methods match the grid to the interface location at every time-step; however, these methods can have difficulty resolving highly distorted interfaces and waves [20]. Interface-capturing methods use techniques that do not require altering the domain grid, but because of this, these techniques can cause the sharpness of the interface to be dependent upon the grid resolution and discretization schemes that are used. Some interface-capturing techniques include the marker-and-cell method [21], the level set method [22], and the volume of fluid (VOF) method [23]. Marker-and-cell or marker particle methods can be very robust, but often have a high computational cost, level set methods can have issues with accuracy when the interface is significantly deformed, and some VOF methods can suffer from artificial (numerical) coalescence of gas bubbles [24]. In VOF methods, the use of a high-resolution interface-capturing (HRIC) scheme can help maintain a sharp interface [25].

The VOF method has proven useful in past studies for multiple types of free surface and bubbling flows [24,26-28] and is utilized here with the HRIC scheme.

In this paper, CMFD is used to investigate the heat transfer dynamics of the small-scale DM100 melter. A three-phase VOF method is used for the separation and interface tracking of the primary physical regions of the melter. The overarching goal is that through the simulation and validation of the DM100 melter, a greater level of confidence can be placed in future melter models, including the pilot scale DM1200 and the full scale WTP. The process of building this validation hierarchy is similar to the procedure outlined by Oberkampf and Roy [29].

2. THEORY

The STAR-CCM+ 10.06.010-R8 commercial software package is used for the CMFD simulations. The Eulerian multiphase VOF approach is used for modeling the different phases of the melter system; the formulation of the governing equations that are used is according to the implementation in the commercial code [30]. The VOF approach estimates the phases as a single effective fluid where the local fluid properties are dictated according to the volume fraction of each individual fluid α_i, defined as

$$\alpha_i = \frac{V_i}{V} \tag{1}$$

where V_i is the volume of fluid i, and V is the volume of the cell; here i = 3 for the molten glass, cold cap and gas phases. In integral form, the mass conservation equation for the volume fraction of fluid i is given by

$$\frac{\partial}{\partial t}\int_V \alpha_i \mathrm{d}V + \int_S \alpha_i(\mathbf{v} - \mathbf{v_g}) \cdot \mathrm{d}\boldsymbol{S} = \int_V \left(s_{\alpha_i} - \frac{\alpha_i \mathrm{D}\rho_i}{\rho_i \mathrm{D}t}\right)\mathrm{d}V \tag{2}$$

Here, s_{α_i} represents any source terms, ρ_i is the specific fluid density and $\mathbf{v}$ and $\mathbf{v_g}$ are the fluid and relative grid velocities. The volume fractions of the fluids are constrained by the simple condition, $\sum_i \alpha_i = 1$. Through combining and rearranging the individual conservation equations, the integral form of the overall mass conservation can be expressed as

$$\int_S (\mathbf{v} - \mathbf{v_g}) \cdot \mathrm{d}\boldsymbol{S} = \sum_i \int_V \left(s_{\alpha_i} - \frac{\alpha_i \mathrm{D}\rho_i}{\rho_i \mathrm{D}t}\right)\mathrm{d}V \tag{3}$$

The main flow parameters that characterize the bubbling flow in the glass phase are the density, viscosity and surface tension. For the air phase, an ideal gas law is used for the density, for the molten glass a temperature dependent linear profile is used, and for the cold cap layer a piecewise temperature dependent density is used. For the fluid-averaged properties, simplistic functions are used due to the flow characteristics being far from a dispersed bubbling regime. For the density and viscosity of the mixture a volume-averaged approach is used, and for the heat capacity of the mixture a mass-averaged approach is used.

The viscosity of the glass is assumed to be a constant 5.0 Pa•s [8]. The viscosity of the cold cap is assumed to be an effective viscosity to account for the porosity of the layer without modeling the small bubbles. This makes it a strong function of temperature as the bubbles form, coalesce and escape; a study on the viscosity has been performed to build an equation to empirically fit experimental data [14]. The equation is given by

$$\eta_{CC} = \begin{cases} 1000\ Pa \cdot s, & if\ T \leq 525℃ \\ \exp\left(-7.5936 + \dfrac{11438}{T}\right), & if\ T \leq 1000℃ \\ \exp\left(-5.0995 + \dfrac{8298}{T}\right), & \text{otherwise} \end{cases} \quad (4)$$

At low temperatures, a constant viscosity is prescribed rather than extrapolating the correlation. This approximation enables better convergence of the pressure and velocity solvers using the 3-fluid VOF, and may be revisited in future studies. The three fluid phases are assumed to be immiscible. The molecular forces at the interface between immiscible fluids create a surface force at the interface relative to the surface tension, σ. For the simulations the surface tension is an interface-normal force of [31]

$$f_{\sigma,n} = \sigma\kappa\nabla\alpha_i \quad (5)$$

Where κ is the curvature of the fluid interface, expressed as

$$\kappa = -\nabla \cdot \frac{\nabla\alpha_i}{|\nabla\alpha_i|} \quad (6)$$

For the simulations here, it is assumed that the surface tension is constant with respect to temperature and other parameters, which results in the tangential component of the surface force equaling zero. For the surface tension a constant value of 0.3 N/m is used for the glass phase [8]. For the surface tension of the cold cap, no experimental studies have been performed. It is assumed that the surface tension has the same magnitude as that of the molten glass. In the CMFD code, the HRIC scheme is used for tracking the interfaces between each of the three fluids [25]. The HRIC blends differencing schemes in a way that keeps a sharp fluid interface while maintaining numerical stability [30].

In the cold cap layer, rapid temperature gradients occur, as well as changes to the morphology and composition of the layer as the feed-to-glass reaction proceeds. Various experiments were carried out at the lab-scale to give insight into the properties that can be used to model the cold cap [13,32]. In these studies, the cold cap can be expressed as a combined medium consisting of a porous and a primary foam phase, but the physical parameter models are constructed to be continuous across the phases. With a simplification for the CMFD implementation of the cold cap phase, it is considered as a single liquid VOF phase with a variable density based on the temperature. The variable density is built to model an “effective” density to account for the density changes in the phase between the porous and foamy layers. Pellet expansion tests on the feed stream have been used to correlate the density as a function of temperature as the feed-to-glass conversion occurs [11]. The porosity of the cold cap region will also cause the density of the effective fluid to change as a function of temperature as well. An empirical correlation has been developed for the density as it changes in the different layers of the cold cap [11].

A constant glass thermal conductivity of 5.0 W/(m K) at 1423K was assumed since the glass pool temperature does not vary greatly. The thermal conductivity of the cold cap was determined by matching a one-dimensional solution of the partial differential equation for temperature to experimental measurements of a small batch melter, applied to the observed cold cap foamy structure [12,13]. The expression for the thermal conductivity of the cold cap phase is

$$k_{CC} = \begin{cases} 0.311 - 1.06\text{e-}4\ T, & if\ T \leq 700℃ \\ -6.9164 + 0.0102\ T, & if\ T \leq 800℃ \\ 0.5\ \mathrm{W/(m\ K)}, & otherwise \end{cases} \quad (7)$$

For the heat capacity of the cold cap layer, the value was fitted as a complex function of temperature to thermogravimetric analysis (TGA) data given by Rodriguez et al. [16], in a similar manner as the one-

dimensional model [11]. The primary heating of the glass melt pool is provided through ohmic (or Joule) heating via electric currents. The amount of energy provided from the Joule heating can be expressed as

$$Joule\ Heat = \boldsymbol{E} \cdot \boldsymbol{J} \tag{8}$$

where $\boldsymbol{E}$ is the electric field and $\boldsymbol{J}$ is the electric current. For the glass phase a constant electrical conductivity of 30 S/m is used [36]. For the cold cap layer, components of the glass are often mixed with water prior to being feed into the melter, so it was assumed to use the electrical conductivity of water of 5.5e-6 S/m. For the gas phase, the electrical conductivity of air was used. To account for the radiative heat transfer, a weighted sum of grey gases was comprised of water vapor and carbon dioxide in the plenum region [37].

For these simulations, in an effort to isolate the heat transfer effects, the mass addition from the cold cap into the evolved gas and glass phases was ignored. It is assumed the reactor is in a near-steady state operation without the addition of new feed. Due to the slow conversion rate to glass, this is a valid assumption over short timescales. In future validation studies, mass addition from the cold cap layer into the gas and glass phases will be incorporated.

3. SIMULATION SETUP

This study focuses on the small-scale DM100 melter. The horizontal cross-section of the melt pool in the DM100 is 0.3556 m x 0.3038 m, which yields a surface area of 0.108 m^2. There is a large 0.4572 m x 0.6096 m plenum region above the melt region. Two pairs of electrodes on opposite sides of the melter provide heating to the glass, another electrode is located on the bottom, but is not powered for these cases. The electrodes span the width of the melter and are each 0.0254 m thick. A schematic for the DM100 melter is shown in Figure 1a [5]. In the CMFD simulations, the computational domain consists of the interior region of the melter as shown in Figure 1b. It includes the melt pool, the plenum region, and the two pairs of electrodes. The DM100 melter is surrounded by a large insulated refractory, so all walls of the CMFD domain are set to zero gradient temperatures. The CMFD mesh has a total of 5.3 million cells with a base size of 0.01 m, and a finer volume resolution of 0.0025 m used in the cold cap and bubbling regions.

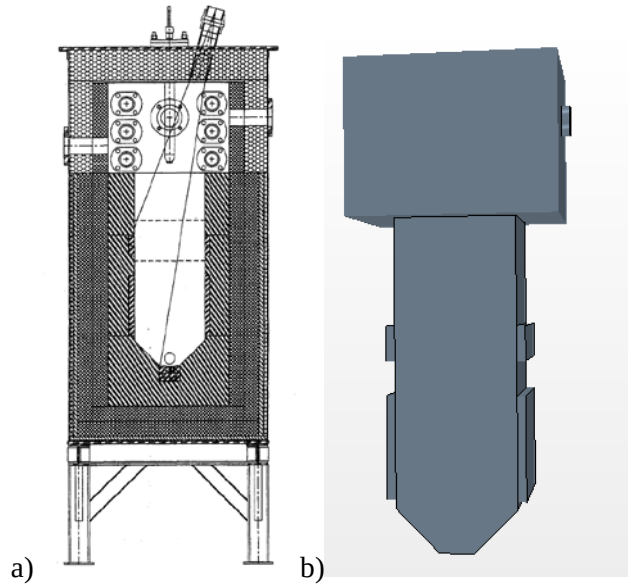

a) b)

Figure 1. Schematic of the (a) side view of the DM100 melter [5] and (b) corresponding CMFD domain.

In the study by Dixon et al. [33], the cold cap was sectioned after the completion of a small batch melter experiment. By analyzing the microstructures of the quenched cold cap, temperature distributions were approximated in order to derive an empirical correlation for the temperature as a function of the cold cap height. In the lab-scale study, the cold cap had a thickness of approximately 20 mm [33]. In the DM100, the cold cap is considerably thicker, at around 0.1524 m; the correlation from Dixon et al. [33] was altered to scale with the size of the cold cap such that most of the temperature gradient occurs in the lower one inch of the cold cap. The upper portion of the cold cap consists of the majority of the layer and is set to a constant temperature of 673 K. The melt rate of the cold cap is neglected, as over the short timescales of the simulations, this contribution to the total glass pool present should be small.

The plenum region above the cold cap was also initialized to a temperature of 673 K, and the molten glass region was initialized to a temperature of 1423 K. The electrodes were initialized to a temperature of 1423 K, and were given a constant voltage across the DM100 melter of 30.7 V for simplicity across the simulations. While the experiments exhibit fluctuations in electrode power, in the simulations the voltage was kept constant. It is assumed that the melter operates at steady-state.

The melt region has a tall, slender geometry with a depth of 0.9779 m and a glass loading height initialized to 0.7366 m. The cold cap layer is reported to be between 6 to 8 inches thick (Innocent Joseph, personnel communication, VSL, March 14, 2016), therefore a 0.1524 m (6 inches) thickness was used in the model. The cold cap was initialized in a block covering about 80% of the glass surface area. The initialized volume fraction of the phases and the temperature for the computational domain is shown along the centerline slices in Figures 2a and 2b. For the volume fraction, the blue is molten glass, the green is the cold cap and the red is the gas phase. The initial temperature distribution shows the constant temperatures in the plenum, upper cold cap and molten glass regions, and the applied temperature gradient profile in the cold cap.

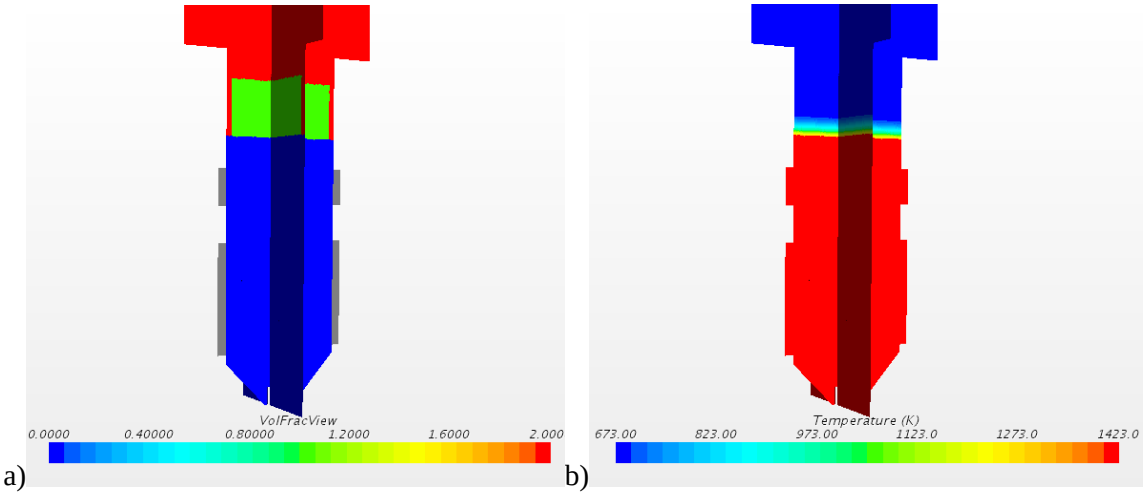

a) b)

Figure 2. Initialized CMFD domain for (a) volume fraction and (b) temperature.

At the VSL, experiments for the DM100 were run at various air bubbling rates to test the effect of bubbling on the total glass conversion rates. Three of those tests were examined here, with bubbling rates ranging over two orders of magnitude. The experimental bubbling flow rates are given in Table 1. The experiments were run for long time periods ranging from 56 hours up to 120 hours. To resolve the phase interfaces for the bubbling in the CMFD code, it is infeasible to run simulations for the large timescales of the full experiments. While this presents a limitation, the resolution of the bubbling flow here should provide better insight into the interaction of bubbles with the cold cap than using an averaged Stokes flow velocity with a momentum source term approach as done by Choudhary et al. for a commercial melter [38].

Table 1. Flow rate test summary. [3]

VSL Test Number	Bubble flow rate (kg/s)
2	9.440×10^{-7}
5	1.888×10^{-5}
8	1.130×10^{-4}
9	4.719×10^{-5}

Here, the selected tests were done using only the nominal feed, so that only flow rates are varied between the tests. It is assumed that this feed has the same thermal properties of the high level waste feed that has been reported elsewhere [11-19], even though the exact composition is slightly different. Ideally, the CMFD model provides a platform to explore the sensitivities of the various parameters on heat transfer within the melter. The results are useful to inform the cold cap modeling effort [11]. A diagram illustrating the various modes of heat transfer occurring in the melter is shown in Figure 3. Rising bubbles induce convective currents, the electrodes provide Joule heating, and radiation from the openings in the cold cap provide heat to the plenum, which in turn provides heat to the top of the cold cap. Thus, heat is provided to drive the chemical reactions occurring in the cold cap. These reactions serve to convert the feed to glass [32].

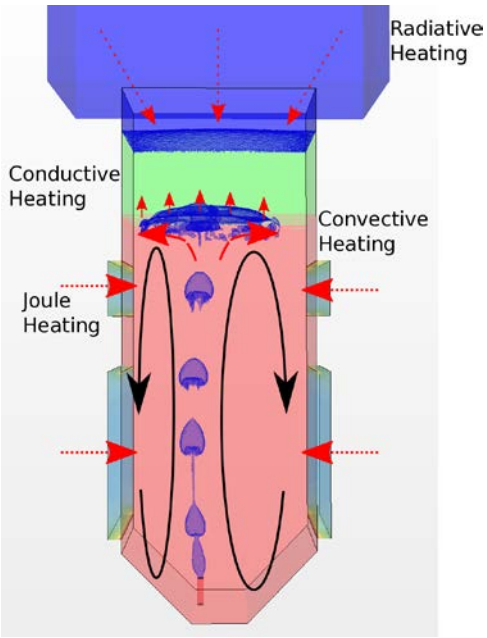

Figure 3. Diagram of heat transfer effects in the melter, coloring illustrates the gas (blue), cold cap (green) and glass regions (pink).

4. RESULTS AND DISCUSSION

The timescales for the heating of the glass with respect to the timesteps required to resolve the leading edge of the air bubbles makes it unfeasible to use the molten glass thermocouples for validation in cases with high bubbling rates. For the plenum region, while the temperatures vary on shorter timescales, direct comparisons with the experimental data are not possible. The plenum temperature is controlled by the cold cap coverage, and is thus dependent upon the feeding and melting rates. Moreover, the plenum temperatures for the older experiments are reported only as a function of time with no cold cap coverage observations. The time between the maximum and minimum points in the data are on timescales of hours, which again are not typical for CMFD timescales that require a more refined time resolution to model the free surfaces. Here, the numerical values for the different components of the heat transfer are evaluated as a parametric study against the bubbling rate of the system and the system is assumed to be at a quasi-steady state once several bubbles impact the cold cap, and values such as interfacial surface area, and heat transfer start to plateau.

First, the simplest dynamic of the system is studied, which is the Joule heating of the glass from the electrodes. Figure 4 shows the electrical potential field, the electric current magnitude and the corresponding heat source in a slice of the domain for 2. The electric potential shows a nearly linear field from the positive to negative electrodes, with distortions mainly occurring due to the uneven bubbles and cold cap surface. The electrical current is concentrated near the electrodes and shows very little conductivity into the cold cap, as would be expected due to the low electrical conductivity that was assumed. The ohmic heat source shows the volumetric heating rate from the electrodes in the molten glass, the concentration is directly correlated with the current density, and shows that the heating only affects the glass, and not the rising bubbles. The ohmic heat source is integrated over the entire volume of the glass melt and calculated to be 14.40 kW. For the other cases here, the integrated value of the ohmic heat source varied less than 1% from this value. Of course, this would vary more in the experiments as the power across electrodes is adjusted.

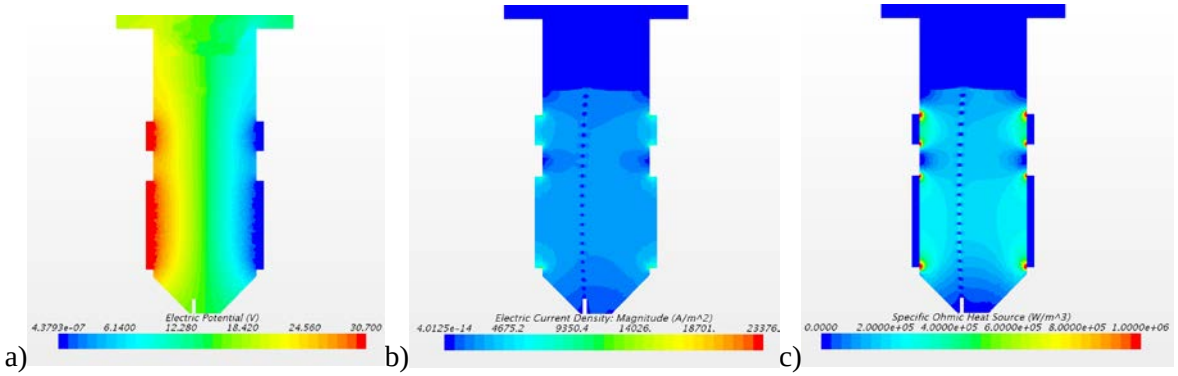

a) b) c)

Figure 4. A slice of the domain showing the (a) electric potential, (b) electrical current density, and (c) the heat source from Joule heating.

The bubbler inserted into the bottom of the melter induces forced convection currents. The flow rate and size of the bubbles effects the strength of the convective currents, and will also influence the interactions between the molten glass and cavities at the cold cap bottom. Images of the bubbling in the different flow rate cases are shown in Figure 5. The red color is the gas, the blue is the molten glass and the green is the cold cap region. In general, increasing the bubbling rate causes bubbles to grow larger near the inlet before buoyancy causes detachment and lifting from the bubbler nozzle. The model shows the bubbles gathering beneath the cold cap and some gas escaping around the sides.

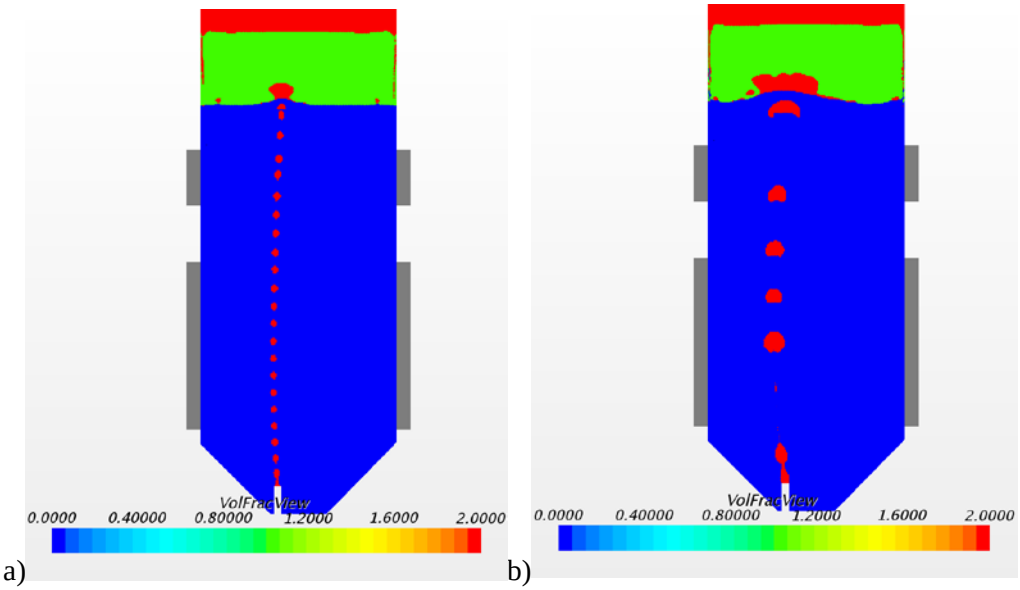

a) b)

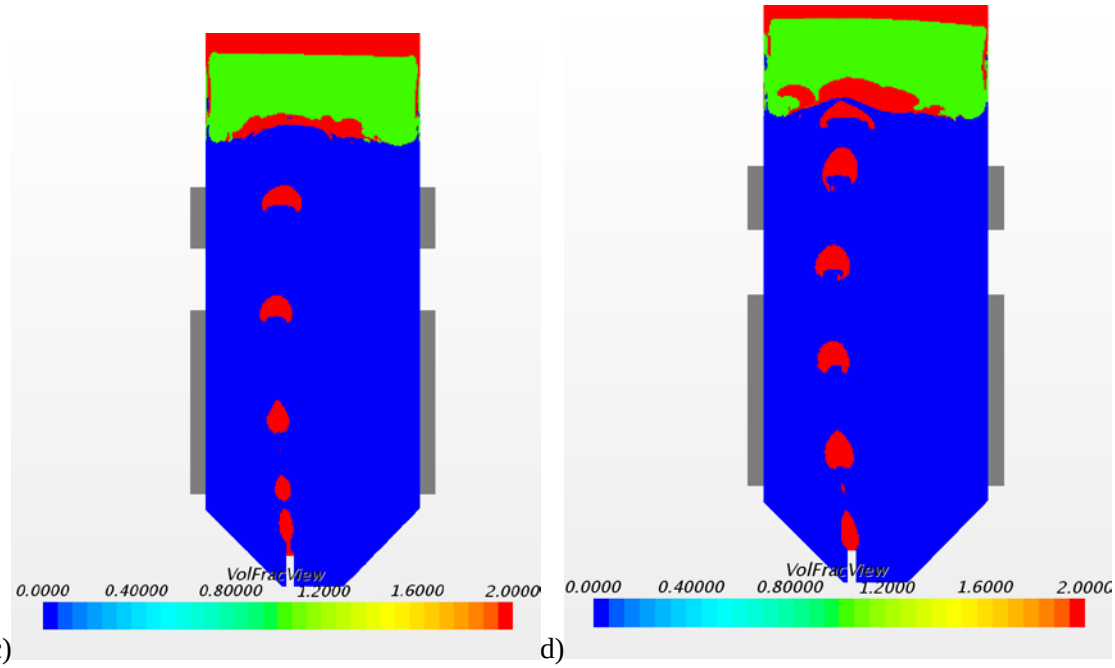

c) d)

Figure 5. Rising bubbles in the melter which are trapped after penetrating the less viscous layer for air injection rates of (a) 9.44x10^{-7}, (b) 1.888x10^{-5}, (c) 4.719x10^{-5}, and (d) 1.13x10^{-4} kg/s after about 10 seconds of simulation time.

The diameter of the bubbles is measured near the top of the molten glass layer for each of the cases; the average bubble diameter from the simulations is shown in Figure 6a. The bubble diameter affects the terminal velocity and more importantly the strength of the convective currents. The bubble diameter from the CMFD results can also be compared to a predicted departure diameter of the bubble. A simple approximation for the diameter of hemispherical bubbles is given by [8]

$$D = \sqrt[3]{\frac{12Q}{\pi f}} \tag{9}$$

where Q is the volumetric flow rate, and f is the bubbling frequency. This correlation is also included in Figure 6a. If using a steady state approach with this diameter as the estimate, the actual diameter of the bubbles would be significantly underestimated. A comparison of the results of the correlation for Stokes flow from Choudhary et al. [38] and a correlation for non-Stokes flow given by the modified Davies-Taylor correlation [39] for these bubble sizes is shown in Figure 6b. The Stokes flow equation is given by

$$U_t = \frac{2r_b^2 \rho_l g}{9\mu_l} \tag{10}$$

and the modified Davies-Taylor correlation is given by

$$U_t = 1.02\sqrt[2]{gr_b} \tag{11}$$

The averaged velocities for the rising bubbles after the quasi steady-state is reached are also plotted in Figure 6b. The data from the simulation shows better agreement with the modified Davies-Taylor correlation than the Stokes flow velocity.

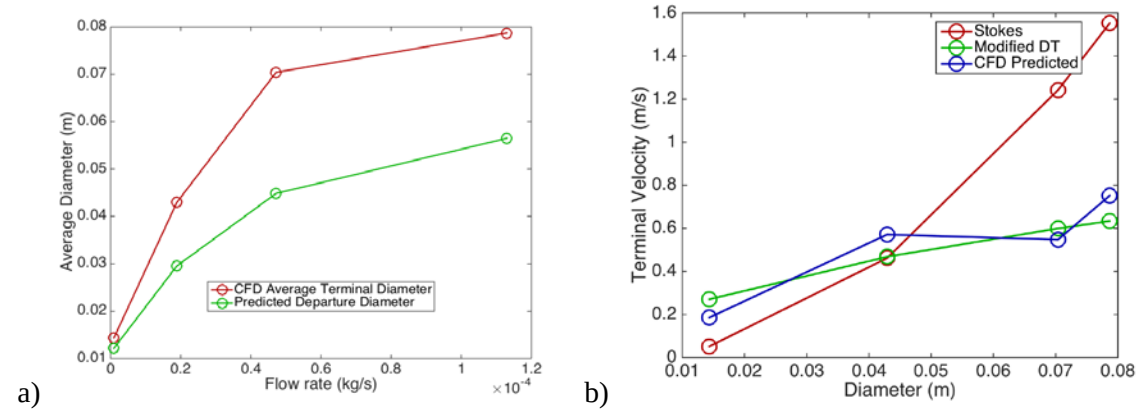

Figure 6. (a) Average bubble diameter as a function of injected air flow rate, and (b) bubble terminal velocity as a function of bubble diameter.

The rising bubbles will also have an indirect effect on the heat transfer between the molten glass and the cold cap. While the experimental data does not provide a direct measurement of the influence of bubbling on the cold cap, the 3D CMFD model provides the ability to assess the heat transfer to the cold cap layer. The interface is defined as computational cells where the volume fraction of the cold cap is equal or interpolated to 0.5 in the volumetric region of interest. At the bottom of the cold cap the local temperature gradient is used to estimate the heat transfer coefficient. The spatially averaged heat transfer coefficient is plotted in Figure 7 as a function of the bubbling flow rate. The higher convection currents near the surface create higher local gradients used in the calculation of the heat transfer coefficient.

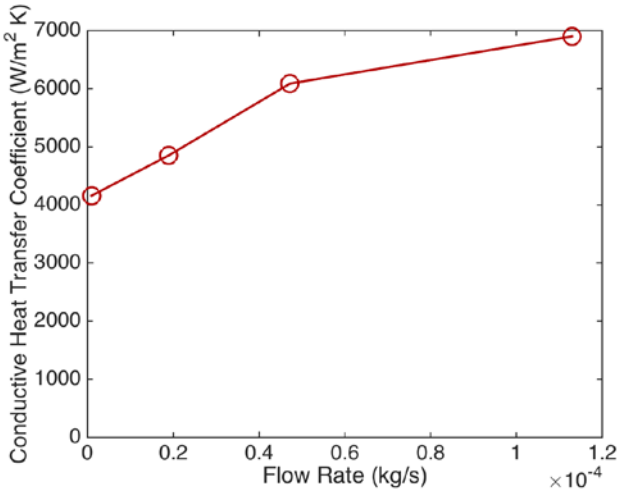

Figure 7. Spatially averaged heat transfer coefficient as a function of bubbling rates.

The governing equations are solved for the entire melter as a single computational domain, rather than by separate models [40]. The plenum above the cold cap is heated though a combination of escaping gases and radiation through the vent holes and gaps in the cold cap layer. The heat in the plenum then subsequently provides heating at the top of the cold cap layer. From the various heat fluxes occurring in the system, which affect the cold cap, the temperature of the bottom of the cold cap interface can be calculated. As discussed previously, the cold cap interface is defined where the volume fraction of the cold cap is equal or interpolated to 0.5. The surface averaged temperature profile is shown in Figure 8. As with the heat transfer coefficient, an increase in the temperature at quasi-steady state is seen with an increase in bubbling rate.

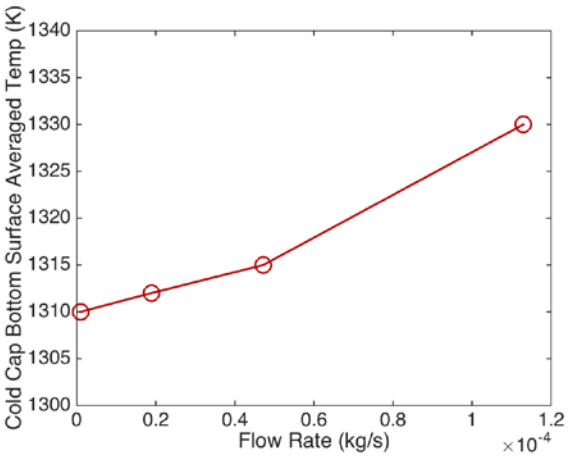

Figure 8. Cold cap bottom surface spatially averaged temperature.

Figure 9 shows the integrated shear rates that are calculated at the interface between the glass and the cold cap. The higher shear rates should help to displace gas cavities in the lower portion of the cold cap. The displacement of cavities due to bubbling causes better heat transfer from the glass into the bottom of the cold cap, and in a fully coupled system would also increase melt rates.

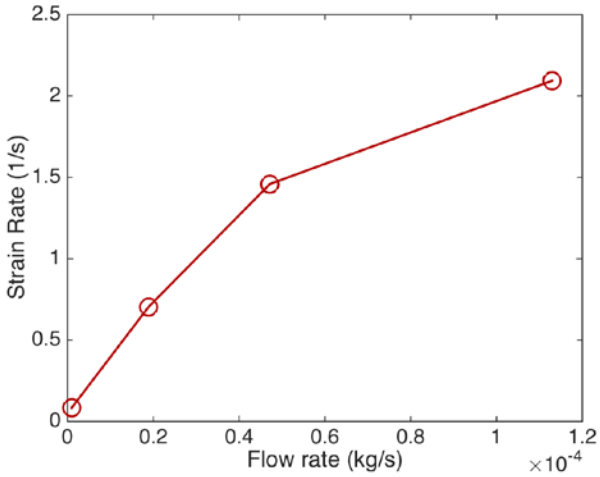

Figure 9. Integrated shear rates at the cold cap bottom surface.

While no conversion rate has been implemented into the CMFD simulation to obtain accurate point wise reaction rates, eventually coupling the CMFD model with advanced cold cap models [10] should provide an accurate description of the melting rate. The overall melt rates for these experimental tests are listed in Table 2 [3]. As one would expect from the melting rates shown, the increase in bubbling rates should cause an increase in the predicted melt rate, which is in qualitative agreement with the results presented above. The quantitative agreement should be achieved once the full cold cap model (including reaction kinetics and foam dynamics) is coupled with the melter model.

Table 2. Overall melt rates from the experimental data (kg/m^2/day). [3]

No.	Steady State Average (kg/m^2/day)
2	430
5	650
8	1300
9	800

5. CONCLUSIONS AND FUTURE WORK

This study examined the heat transfer effects of bubbling in a small-scale waste glass melter using a CMFD model of the DM100 melter. The parameters for modeling the different phases of the melter were derived from experimental studies on individual aspects of the system. The bubbling rate of the melter was increased across the tests, with other variables held constant. Overall, the simulations show that the higher bubbling flow rates lead to a higher rate of heat transfer into the reactive cold cap region due to increased glass-cold cap interface temperature and other effects, such as higher shear rate helping to displace the cavities at the cold cap bottom. This in turn should lead to higher reaction rates in the cold cap. However, these results are only qualitative at this point, and further validation of the CMFD model and its coupling with the full cold cap model is needed in order to achieve qualitative prediction capabilities of the final melter model.

ACKNOWLEDGMENTS

This manuscript was authored by Battelle Energy Alliance, LLC under DOE Contract No. DE-AC07-05-ID14517. Funding was provided by the DOE Office of River Protection, Waste Treatment and Immobilization Plant Project under the direction of Albert A. Kruger.

REFERENCES

1. P. Hrma, “Conversion of nuclear waste into nuclear waste glass: Experimental investigation and mathematical modeling,” 2nd International Summer School on Nuclear Glass Wasteform: Structure, Properties and Long-Term Behavior, SumGLASS 2013, *Procedia Materials Science*, **7**, pp. 117-123, (2014).
2. C. Chapman, “Modeling the HLW Melter with Revised Bubbler Design and Noble Metals,” REP-PLT-069, Rev. 0, Duratek, Inc., Richland, Washington, September 26, (2005).
3. K.S. Matlack, A.A. Kruger, W.K. Kot, and I.L. Pegg. “Final Report Melter Tests with AZ-101 HLW Simulant Using a DuraMelter 100 Vitrification System,” The Catholic University of America, Vitreous State Laboratory, VSL-01R10N0-1, Rev. 1, February 25, (2002).
4. K.S. Matlack, A.A. Kruger, W. Gong, I.L. Pegg. “Final Report DuraMelter HLW Simulant Validation Tests with C-106/AY-102 Feeds,” The Catholic University of America, Vitreous State Laboratory, VSL-05R5710-1, Rev. 0, June 2, (2005).
5. A.A. Kruger, K.S. Matlack, W. Kot, I.L. Pegg, M. Chaudhuri, and W. Lutze. “Final Report – Effects of High Spinel and Chromium Oxide Crystal Contents on Simulated HLW Vitrification in DM100 Melter Tests,” The Catholic University of America, Vitreous State Laboratory, VSL-09R1520-1, Rev. 0, June 22, (2009).
6. K.S. Matlack, G. Diener, T. Bardakci, and I.L. Pegg, “Summary of DM1200 Operation at VSL Final Report,” The Catholic University of America, Vitreous State Laboratory, VSL-06R6710-2, Rev. 0, September 7, (2006).
7. K.S. Matlack, H. Gan, M. Chaudhuri, W. Kot, W. Gong, T. Bardakci and I.L. Pegg. “Final Report DM100 and DM1200 Melter Testing with High Waste Loading Glass Formulations for Hanford High-Aluminum HLW Streams,” The Catholic University of America, Vitreous State Laboratory, VSL-10R1690-1 Rev 0, August 16, (2010).
8. R.K. Mohr, C.C. Chapman, and I.L. Pegg, “High-Level Waste Melter Alternate Configuration Testing,” The Catholic University of America, Vitreous State Laboratory, VSL-04R4800-3, Rev. 0, June 18, (2004).
9. D.P. Guillen and A. Abboud, Computational Fluid Dynamics Modeling of Bubbling in a Viscous Fluid for Validation of Waste Glass Melter Modeling, Advances in Thermal Hydraulics 2016, New Orleans, LA, June 12-16, 2016.
10. B.C. Hodges, D.C. Iverson and G. Diener, “Operation of bubblers in the savannah river site defense waste processing facility melter, Paper 12166,” *Waste Management WM2012 Conference*, Phoenix, AZ, USA, February 26 – March 1, (2012).

11. R. Pokorny, Z.J. Hilliard, D.R. Dixon, M.J. Schweiger, D.P. Guillen, A.A. Kruger and P. Hrma. "One dimensional cold cap model for melters with bubblers," *Journal of American Ceramic Society*, **98**(10), pp. 3112-3118, (2015).
12. J.A. Rice, R. Pokorny, M.J. Schweiger, and P. Hrma. "Determination of heat conductivity and thermal diffusivity of waste glass melter feed: extension to high temperatures," Journal of American Ceramic Society, **97**(6), pp. 1952-1958, (2014).
13. R. Pokorny, J.A. Rice, M.J. Schweiger, P. Hrma. "Determination of temperature dependent heat conductivity and thermal diffusivity of waste glass melter feed," Journal of American Ceramic Society, **96**(6), pp. 1891-1898, (2013).
14. J. Marcial, C. Jaehun, P. Hrma and M. Schweiger. "Effect of bubbles and silica dissolution on melter feed rheology during conversion to glass." *Environmental Science and Technology*, **48**, pp. 12173-12180, (2014).
15. R. Pokorny, D. A. Pierce and P. Hrma, "Melting of glass batch: Model for multiple overlapping reactions," *Thermochimica Acta*, **541**, pp. 8-14, (2012).
16. C.P. Rodriguez, J. Chun, M.J. Schweiger, A.A. Kruger, and P. Hrma, "Application of evolved gas analysis to cold-cap reactions of melter feeds for nuclear waste vitrification," *Thermochimica Acta*, **592**, pp. 86-92, (2014).
17. J. Chun, D.A. Pierce, R. Pokorny, and P. Hrma. "Cold-cap reactions in vitrification of nuclear waste glass: Experiments and modeling," *Thermochimica Acta*. **559**, pp. 32-39, (2013).
18. D.P. Guillen, and C.J. Beers, "Modeling the vitrification of Hanford tank waste," *Transactions of the American Nuclear Society*, Vol. **112**, June (2015).
19. R. Pokorny, A.A. Kruger and P. Hrma, "Mathematical modeling of cold cap: Effect of bubbling on melting rate," *Ceramics-Silikaty*, **58**(4), pp. 296-302, (2014).
20. S.H. Rhee, B.P. Makarov, H. Krishinan and V. Ivanov, "Assessment of the volume of fluid method for free-surface wave flow," *Journal of Marine Science and Technology*, **10**, pp. 173-180, (2005).
21. E.H. Harlow and J.E. Welch, "Numerical calculation of time-dependent viscous incompressible flow with free surface," *Physics of Fluids*, **8**, pp. 2182-2189, (1965).
22. M. Sussman, P. Smereka and S. Osher, "A level set approach for computing solutions to incompressible two-phase flow," *Journal of Computational Physics*, **114**, pp. 146-159, (1994).
23. C.W. Hirt and B.D. Nichols, "Volume of fluid method for dynamics of free boundaries," *Journal of Computational Physics*, **39**, pp. 201-221, (1981).
24. M. van Sint Annaland, N. G. Deen, and J. A. M. Kuipers, "Numerical simulation of gas bubbles behaviour using a three-dimensional volume of fluid method," *Chemical Engineering Science*, **60**(11), pp. 299-3011, (2005).
25. S. Muzaferija and M. Peric, "Computation of free-surface flows using interface-tracking and interface capturing methods," *Nonlinear Water Wave Interaction*, pp. 59-100, Computational Mechanics Publications, Southampton, UK, (1998).
26. Y. Pan and D. Langberg, "Physical and mathematical modeling investigations of the mechanisms of splash generation in bath smelting furnaces," *Seventh International Conference on CMFD in the Minerals and Process Industries*, Melbourne, Australia, December 9-11 (2011).
27. H.A. Jakobsen, H. Lindborg and C.A. Dorao, "Modeling of bubble column reactors: Progress and limitations," *Industrial and Engineering Chemical Research*, **44**, pp. 5107-5151, (2005).
28. D. Gueyffier, J. Li, A. Nadim, R, Scardovelli, and S. Zaleski, "Volume-of-fluid interface tracking with smoothed surface stress methods for three-dimensional flows," *Journal of Computational Physics*, **152**, pp. 423-456, (1999).
29. W.L. Oberkampf and C.J. Roy, *Verification and Validation in Scientific Computing*, Cambridge University Press, New York USA, (2010).
30. CD-Adapco, User Guide, Star CCM+ Version 10.06.010-R8, (2015).
31. J.U. Brackbill, D.B. Kothe and C. Zemach, "A continuum method for modeling surface tension," *Journal of Computational Physics*, **100**, pp. 335-354, (1992).
32. R. Pokorny and P. Hrma, "Model for the conversion of nuclear waste melter feed to glass," *Journal of Nuclear Materials*, **445**, pp. 190-199, (2014).
33. D.R. Dixon, M.J. Schweiger, B.J. Riley, R. Pokorny, and P. Hrma, "Temperature distribution within a cold cap during nuclear waste vitrification," *Environmental science & technology*, **49**(14), pp. 8856-8863, (2015).

34. D.P. Guillen, “Bubbling in a waste glass melter,” *WIT Transactions on Engineering Sciences*, WIT Press, **89**, (2015).
35. INCONEL alloy 690, Special Metals Corporation, (2009).
36. P. Schill, “Modeling the behavior of noble metals during HLW vitrification,” in: W. Lutze, Modeling the behavior of noble metals during HLW vitrification in the DM1200 melter, VSL-05R5740-1, Vitreous State Laboratory, (2005).
37. G. Krishnamoorthy, “A new weighted-sum-of-gray-gases model for CO2-H2O gas mixtures,” *International Communications in Heat and Mass Transfer*, **37**, pp. 1182-1186, (2010).
38. M.K. Choudhary, R. Venuturumilli, M.R. Hyre. “Mathematical modeling of flow and heat transfer phenomena in glass melting, delivery, and forming processes,” *International Journal of Applied Glass Science*, **1**, pp. 188–214, (2010).
39. H.D. Mendelson, “The prediction of bubble terminal velocities from wave theory,” *AIChE Journal*, **13**, pp. 250-253, (1967).
40. C.C. Chapman and W. Lutze, Computer Simulation Study of the Behavior of Noble Metals in the WTP HLW Melter, The Catholic University of America, Vitreous State Laboratory,VSL-05R5740-2, August 8, (2005).